

High-strength bulk Al-based bimodal ultrafine eutectic composite with enhanced plasticity

Jin Man Park

Leibniz Institute for Solid State and Materials Research Dresden, Institute for Complex Materials, D-01171 Dresden, Germany; and Center for Non-Crystalline Materials, Yonsei University, Seoul 120-749, Republic of Korea

Norbert Mattern and Uta Kühn

Leibniz Institute for Solid State and Materials Research Dresden, Institute for Complex Materials, D-01171 Dresden, Germany

Jürgen Eckert^{a)}

Leibniz Institute for Solid State and Materials Research Dresden, Institute for Complex Materials, D-01171 Dresden, Germany; and TU Dresden, Institute of Materials Science, D-01062 Dresden, Germany

Ki Buem Kim

Department of Advanced Materials Engineering, Sejong University, Seoul 143-747, Republic of Korea

Won Tae Kim

Division of Applied Science, Cheongju University, Cheongju 360-764, Republic of Korea

Kamanio Chattopadhyay

Department of Metallurgy, Indian Institute of Science, Bangalore 560-012, India

Do Hyang Kim^{b)}

Center for Non-Crystalline Materials, Department of Metallurgical Engineering, Yonsei University, Seoul 120-749, Republic of Korea

(Received 23 January 2009; accepted 30 March 2009)

An *in situ* bulk ultrafine bimodal eutectic Al–Cu–Si composite was synthesized by solidification. This heterostructured composite with microstructural length scale hierarchy in the eutectic microstructure, which combines an ultrafine-scale binary cellular eutectic (α -Al + Al₂Cu) and a nanometer-sized anomalous ternary eutectic (α -Al + Al₂Cu + Si), exhibits high fracture strength (1.1 ± 0.1 GPa) and large compressive plastic strain ($11 \pm 2\%$) at room temperature. The improved compressive plasticity of the bimodal-nanoeutectic composite originates from homogeneous and uniform distribution of inhomogeneous plastic deformation (localized shear bands), together with strong interaction between shear bands in the spatially heterogeneous structure.

I. INTRODUCTION

Recently, *in situ* bulk nanostructure-dendrite composites that simultaneously combine high strength and good plasticity have been highlighted because of their unique mechanical properties and easy manufacturing process (simple single step casting).^{1–3} These appealing properties can be introduced by bimodal microstructure distribution with micrometer-sized dendrites embedded in the matrix of nano-/ultrafine-scale eutectics. The high strength is

provided by the nano-/ultrafine eutectic matrix, whereas the enhanced plasticity stems from the inhomogeneous microstructure that suppresses deformation instability.^{4–7} Plastic deformation of these composite materials occurs through a combination of dislocation-based slip in the dendrites and constraint multiple shear banding in the nanostructured matrix.^{8–16}

In this scenario, it is possible to assume that, in general, a bimodal distribution of constituent phases and length scales can be beneficial for the room temperature plastic deformability of high-strength nanostructured materials. However, there have been no studies related to the synthesis and mechanical properties of bimodal ultrafine eutectic composites containing eutectics with different length scales. Moreover, compared with other metallic materials, Al alloys are one of the best lightweight engineering materials for many industrial applications

^{a)}This author was an editor of this journal during the review and decision stage. For the *JMR* policy on review and publication of manuscripts authored by editors, please refer to http://www.mrs.org/jmr_policy

^{b)}Address all correspondence to this author.

e-mail: dohkim@yonsei.ac.kr

DOI: 10.1557/JMR.2009.0297

because of their high specific strength and good corrosion resistance.^{17–20} Therefore, it is worth developing high-strength light alloys, especially Al-rich nano-/ultrafine eutectic composites with high specific strength and large plastic strain at ambient temperature. For this, we selected the simple binary ($\text{Al}_{83}\text{Cu}_{17}$) and ternary eutectic ($\text{Al}_{81}\text{Cu}_{13}\text{Si}_6$) compositions in the Al-rich corner of the respective phase diagrams as starting compositions.²¹

In this study, we present a new class of nanocomposite with length scale hierarchy in the eutectic structure for Al-base alloys, which exhibits enhanced plasticity but also retains high strength at room temperature. Tailoring of the heterostructured nanocomposite has been achieved by appropriate alloy selection and controlled solidification. The high strength of the nanocomposite is attributed to the interlamellar spacing of the constituent eutectics, whereas the large plasticity is from the retardation of shear localization and suppression of the mechanical instability, caused by strong interaction of shear bands within the spatially heterogeneous structure.

II. EXPERIMENTAL

The $\text{Al}_{83}\text{Cu}_{17}$ (alloy I) and $\text{Al}_{81}\text{Cu}_{13}\text{Si}_6$ (alloy II) alloys were prepared by arc melting of the high purity elemental constituents under an Ar atmosphere. Cast samples were produced by injection casting into a cylindrical cavity with 1-mm diameter and 50-mm length. Microstructural analysis of the as-cast and deformed samples was performed by scanning electron microscopy (SEM; S-2700; Hitachi, Tokyo, Japan). X-ray diffraction (XRD; monochromatic Cu K_α radiation, CN2301; Rigaku, Tokyo, Japan) and transmission electron microscopy (TEM; 2100F; JEM, Tokyo, Japan) coupled with energy-dispersive x-ray analysis (EDX; INCA system; Oxford Instrument, High Wycombe, Bucks, UK) were used for structural characterization and phase identification. The TEM samples were prepared by conventional ion milling (Model 600I Gatan, Vienna, OH). The room temperature mechanical properties were evaluated by uniaxial compression tests in an Instron-type machine. Cylindrical specimens with a 2:1 aspect ratio were prepared and tested at a strain rate of $1 \times 10^{-4}/\text{s}$.

III. RESULTS AND DISCUSSION

Figure 1 shows the XRD pattern [Fig. 1(a) inset] and SEM secondary electron micrographs [Figs. 1(a) and 1(b)] of the as-cast alloys I and II. Both alloys exhibited very similar diffraction patterns. The diffraction peaks of alloy I can be identified as a mixture of a face-centered cubic (fcc) α -Al solid solution ($Fm\bar{3}m$, $a = 0.4039 \text{ nm}$) and a body-centered tetragonal (bct) θ phase (Al_2Cu) ($I4/mcm$, $a = 0.6064 \text{ nm}$ and $c = 0.4873 \text{ nm}$).²² For alloy II, weak additional peaks corresponding to a diamond cubic (dc) Si phase ($Fd\bar{3}m$, $a = 0.543 \text{ nm}$) are present

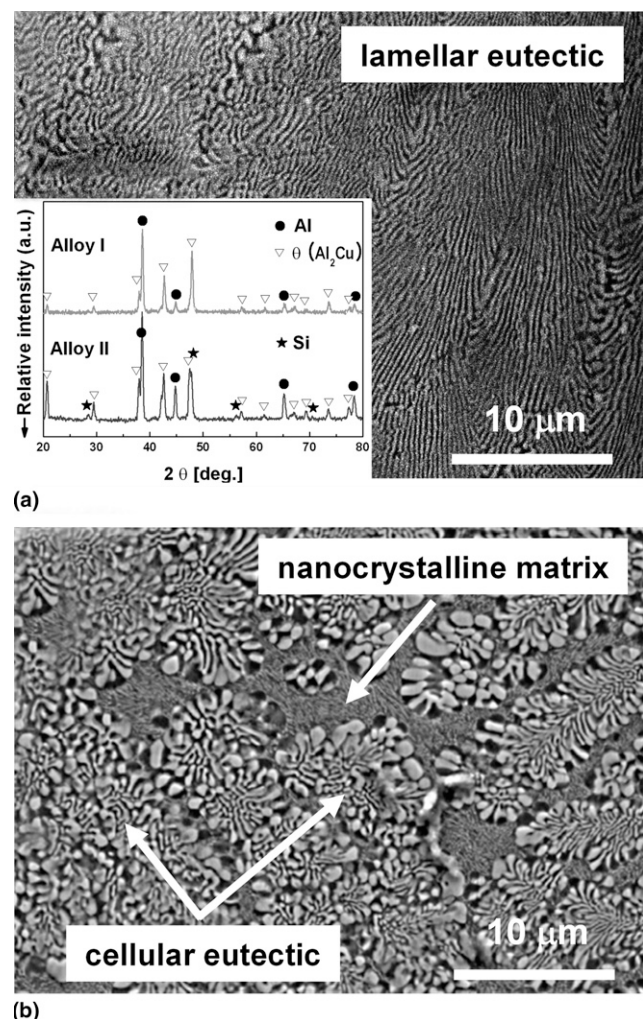


FIG. 1. SEM secondary electron micrographs and XRD patterns of the as-cast alloys I and II: (a) alloy I ($\text{Al}_{83}\text{Cu}_{17}$) and (b) alloy II ($\text{Al}_{81}\text{Cu}_{13}\text{Si}_6$).

besides the reflections of the α -Al solid solution and θ phase (Al_2Cu) phases.²³ The SEM micrograph of alloy I depicted in Fig. 1(a) shows a typical regular lamellar eutectic structure, in which two phases are arranged in an alternating fashion with a lamellar spacing of 200–300 nm. In contrast, alloy II exhibits a significantly different morphology compared with alloy I. As shown in Fig. 1(b), the morphology of the overall microstructure clearly shows a bimodal distribution of the constituent phases with length scale heterogeneity. This inhomogeneity is characterized by the coexistence of a micrometer-sized cellular-type eutectic and a complex nanocrystalline matrix. For the cellular eutectic region with spherical morphology in alloy II, the volume fraction, the average colony size, and the lamellar spacing are 75–85 vol%, 10–20 μm , and 300–700 nm, respectively. EDX analysis shows similar compositions for both the overall lamellar eutectic region (alloy I) and the ultrafine cellular eutectic region (alloy II), whereas the

fine and complex nanostructured matrix region (alloy II) is enriched in Si, indicating the presence of the Si phase in the nanocrystalline matrix. Moreover, analyzing the individual alternating phases within the cellular eutectic region of alloy II shows that the bright phase is enriched in Cu and the dark phase is enriched in Al, respectively. From the structural and phase analyses, one can conclude that the alternating dark and bright phases in the cellular-type eutectic of alloy II are related to the α -Al solid solution and the θ phase (Al_2Cu), respectively, whereas the nanostructured matrix exhibits very fine and complex multiple phases containing the diamond cubic (dc) Si phase.

Figures 2(a)–2(d) show bright field (BF) TEM images and selected-area electron diffraction (SAED) patterns for the as-cast alloys I and II. The BF TEM image in Fig. 2(a), obtained from the as-cast alloy I, shows the regular lamellae with ultrafine scale. The average lamellar eutectic spacing is 200–300 nm, which is in good agreement with Fig. 1(a). The orientation relationship between the two phases in the eutectic has been determined to be $[110]_{\alpha\text{-Al}}/[120]_{\theta}$ and $(111)_{\alpha\text{-Al}}/(211)_{\theta}$.²³ For the as-cast alloy II, the BF TEM image [Fig. 2(b)] presents the complex multimodal eutectic structure containing different length scale eutectics, i.e., the micrometer-sized cellular eutectic (α -Al + θ) and a nanometer-sized anomalous ternary eutectic (α -Al + θ + Si). Moreover, the micrometer-scale cellular eutectic phases are evenly distributed in the nanoscale ternary eutectic matrix. Figures 2(c) and 2(d)

show enlarged views of the regions marked by the squares A (cellular eutectic) and B (nanocrystalline matrix) in Fig. 2(b). The inset SAED patterns correspond to the [110] zone of the fcc structure of the α -Al solid solution and the [120] zone of the bct structure of the θ phase, respectively. Figure 2(d) shows the interlocked ternary eutectic structure showing the size, shape, and distribution of the three phases (bright contrast phase, Si; gray contrast phase, α -Al; dark contrast phase, θ). The inset shows the SAED pattern for the [110] zone of the dc structure of the Si phase. No specific orientation relationship between the α -Al/Si and θ /Si phases can be identified. EDX analysis showed that the average compositions of the α -Al and θ phases in alloy I are $\text{Al}_{97.6}\text{Cu}_{2.4}$ and $\text{Al}_{66.5}\text{Cu}_{33.5}$, respectively. In the case of alloy II, the average compositions of the gray contrast (α -Al), dark contrast (θ), and bright contrast (Si) phases were $\text{Al}_{96.8}\text{Cu}_{2.7}\text{Si}_{0.5}$, $\text{Al}_{63.8}\text{Cu}_{35.4}\text{Si}_{0.8}$, and $\text{Al}_{5.7}\text{Cu}_{6.1}\text{Si}_{88.2}$, respectively, indicating that the solubility of Cu in the Si phase and of Si in the θ phase is very limited and negligible.

Figure 3(a) presents the room temperature engineering stress-strain curves of the as-cast samples and SEM secondary electron micrographs [Figs. 3(b) and 3(c)] taken from deformed samples. Alloy I, which has a completely ultrafine-scale lamellar eutectic structure, exhibits ultrahigh yield (σ_y : 1.0 ± 0.05 GPa) and ultimate fracture (σ_f : 1.2 ± 0.1 GPa) strength with limited plastic strain (ε_p : $\sim 2 \pm 0.5\%$). The yield strength in this study corresponds to the stress level when the

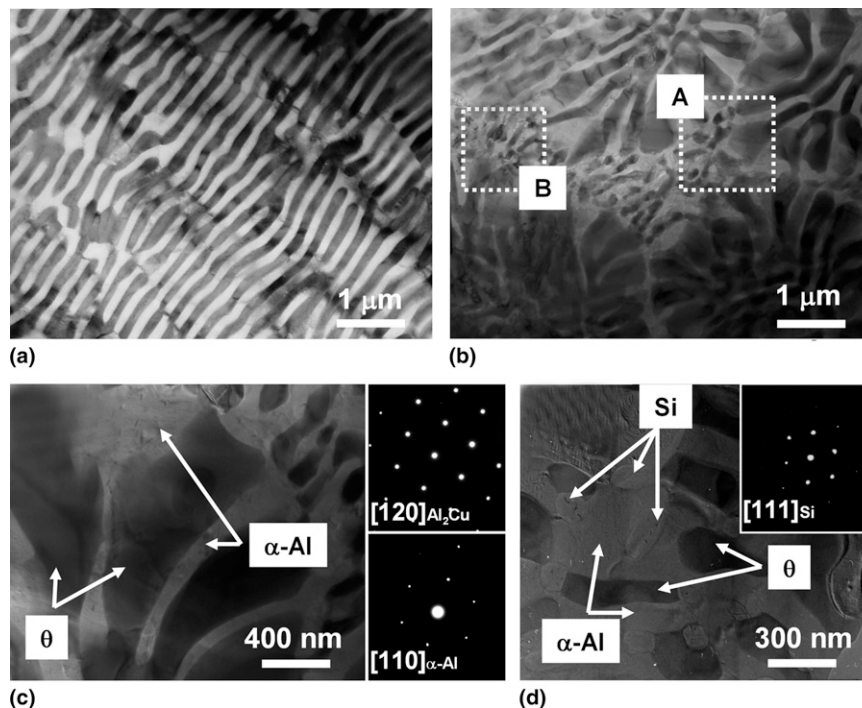


FIG. 2. Bright-field TEM image (a)–(d) and corresponding selected area diffraction patterns of the as-cast alloys I ($\text{Al}_{83}\text{Cu}_{17}$) and II ($\text{Al}_{81}\text{Cu}_{13}\text{Si}_6$).

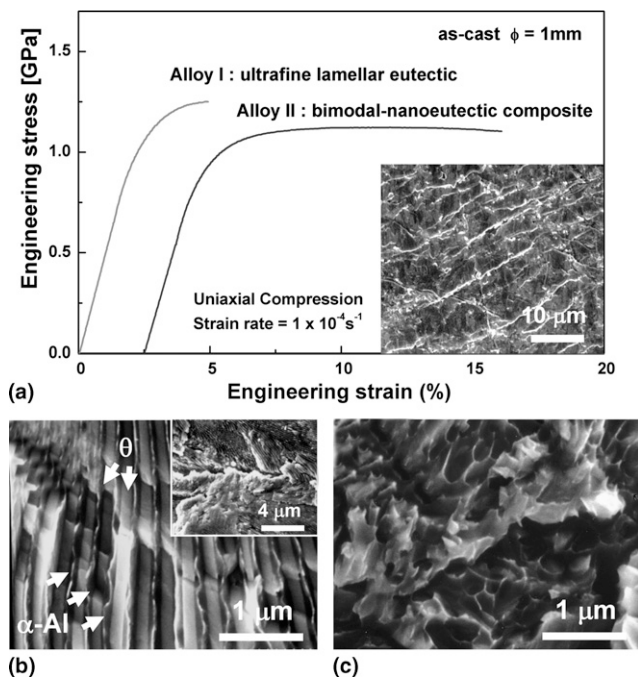


FIG. 3. Room temperature mechanical properties (a) of the as-cast rod samples and SEM secondary electron micrographs (b, c) of failed samples: (a) compressive stress-strain curves, (b) fracture surface of alloy I, and (c) fracture surface of alloy II; the inset in (a) shows the lateral surface morphology of the deformed alloy II.

stress-strain curve deviates from the linear elastic range. On the contrary, alloy II has a lower yield strength (σ_y : 0.8 ± 0.05 GPa) and ultimate fracture strength (σ_f : 1.1 ± 0.1 GPa) but significantly larger plastic strain (ε_p : $\sim 11 \pm 2\%$). However, large size samples (≥ 2 -mm diameter) exhibited relatively reduced mechanical properties, because of the coarsening/modulation of the respective microstructure (Figs. 1 and 2) and introduction of the flaws such as micropores during solidification (not shown). Figures 3(b) and 3(c) show the fracture surface morphologies of the failed samples (alloys I and II), respectively. The fracture surface of alloy I [inset in Fig. 3(b)] with fine lamellar structure shows numerous flat facets with cracks and decohesion of the colony boundary on deformation. It shows cleavage-like features, indicating that the fracture occurred in a brittle manner. Although macroscopic cleavage fracture exists, detailed microscopic observation of individual layers evidently shows that the deformation of the ductile α -Al layers is accompanied by pull-out and softening, whereas the brittle θ (Al_2Cu) layers failed by predominantly sharp-faceted cleavage fracture, as indicated by arrows in Fig. 3(b). On the contrary, as depicted in Fig. 3(c), alloy II shows an apparently changed fracture behavior. The main fracture feature is a rough dimple-like pattern with manifestations of plastic deformation. The inset image in Fig. 3(a) shows the lateral surface of a deformed sample (alloy II). Abundant deformation bands with a spacing of 2–10 μm are homogeneously

distributed over the whole surface region [inset in Fig. 3(a)]. Closer inspection of the lateral and the fracture surfaces of deformed samples (alloy II) shows large deformation before failure. Therefore, it is clear that the bimodal distribution of eutectic phases with different length scale has a strong influence to improve the compressive plastic strain for high-strength Al-based ultrafine eutectic alloys. In view of that, the specific heterogeneous structure should be beneficial to the retardation of shear localization and the suppression of crack nucleation, thus stabilizing more homogeneous overall plastic deformation.

In general, when the growth conditions are not controlled, the final eutectic morphology can be changed toward a dendritic or an anomalous eutectic structure, where the eutectic growth is noncooperative.²⁴ A higher growth rate may render some deviation from the eutectic composition and restrictions of cooperative growth, which leads to primary dendritic phase formation.²⁵ In this study, the formation of the unique heterostructured composite can be explained in terms of the applied nonequilibrium solidification conditions. The relatively high cooling rate (injection casting: $10^2 \sim 10^3$ K/s) and the Si addition destabilize the solid/liquid interface (morphological instability), which is influenced by the topological and crystallographic anisotropy of the two-phase solid/liquid interface, and shift the composition in the coupled zone for the eutectic growth. Thus, the preferential formation of a coupled two-phase univariant cellular eutectic structure and a regular-to-anomalous eutectic morphology transition can occur. Accordingly, the formation of a new class of nanocomposite based on the homogeneous distribution of an inhomogeneous structure with length scale hierarchy (ultrafine-scale cellular eutectic + nanometer-scale anomalous eutectic) is possible.

Considering the correlation of microstructure and mechanical properties, the strength is primarily related to the interlamellar spacing by a Hall-Petch-type relationship,²⁴ whereas the compressive plasticity strongly depends on the microstructural features including the length scale, the volume fraction, and the size and the distribution of the constituent eutectic phases. Hence, the particular heterostructured nanocomposite (alloy II) can effectively release the highly localized shear deformation by generation of multiple shear bands that would otherwise induce catastrophic failure. Furthermore, deformation and fracture behavior are more uniform, and the stress state may become complex, thus leading to an overall homogeneous plastic deformation throughout the whole sample volume. In other words, a spatially homogeneous distribution of heterogeneous structures in nano-/ultrafine-structured materials leads to unique mechanical properties, i.e., enhanced compressive plasticity as well as high strength, by means of preventing inhomogeneous plastic deformation (highly localized shear banding) and inducing overall homogeneous plastic straining (multiple shear banding).²⁶

Our results show that by designing a microstructure with different size scales even in Al-rich, Al-based crystalline alloys, ~ 1.2 GPa and $\sim 11\%$ of strength and plastic strain, respectively, can be obtained in compression. The level of strength is approximately three times higher than for conventional aluminum-based alloys.¹⁷ However, for evaluation of ductility, it is necessary also to conduct tensile tests in which strain localization has a more important role. Because the microstructure of newly developed Al alloys depends on the processing condition, i.e., cooling rate, it is difficult to prepare the novel microstructure with fine scale (Figs. 1 and 2) in relatively larger or standard tensile samples. Moreover, the injection cast samples in larger dimensions suffers from casting defects such as porosity, thus obstructing the suitable tensile testing for this study. Nevertheless, obtaining strength on the GPa level for ductile Al alloy (Al-rich)-based on eutectics in compression is nontrivial and potentially interesting. Therefore, it is believed that this result will have a great impact on the research field of advanced metallic alloy development.

IV. CONCLUSIONS

A novel bimodal nano-/ultrafine eutectic composite ($\text{Al}_{81}\text{Cu}_{13}\text{Si}_6$) with different length scale eutectic phases containing an ultrafine-scale binary eutectic and a nanometer-scale ternary eutectic was prepared using a simple single-step solidification process. The extraordinary room temperature mechanical properties combining high specific strength and large compressive plasticity are caused by the favorable specific heterogeneous microstructure.

ACKNOWLEDGMENTS

The authors thank Dr. J. Jayaraj (IFW-Dresden) for valuable discussions. This work was supported by the Global Research Laboratory Program of the Korea Ministry of Education, Science, and Technology. Additional funding was supported under the AFOSR Task: Basic Research for AOARD 084013 (Dr. Kumar V. Jata, Program Manager).

REFERENCES

1. G. He, J. Eckert, W. Löser, and L. Schultz: Novel Ti-base nanostructure-dendrite composite with enhanced plasticity. *Nat. Mater.* **2**, 33 (2003).
2. J.M. Park, S.W. Sohn, T.E. Kim, K.B. Kim, W.T. Kim, and D.H. Kim: Nanostructure-dendrite composites in the Fe-Zr binary alloy system exhibiting high strength and plasticity. *Scr. Mater.* **57**, 1153 (2007).
3. D.V. Louzguine, H. Kato, and A. Inoue: High-strength hypereutectic Ti-Fe-Co bulk alloy with good ductility. *Philos. Mag. Lett.* **84**, 359 (2004).
4. E. Ma: Controlling plastic instability. *Nat. Mater.* **2**, 7 (2003).
5. J.M. Park, T.E. Kim, S.W. Sohn, D.H. Kim, K.B. Kim, W.T. Kim, and J. Eckert: High strength Ni-Zr binary ultrafine eutectic-dendrite composite with large plastic deformability. *Appl. Phys. Lett.* **93**, 031903 (2008).
6. H. Ma, L.L. Shi, J. Xu, and E. Ma: Chill-cast in situ composites in the pseudo-ternary $\text{Mg}-(\text{Cu},\text{Ni})-\text{Y}$ glass-forming system: Microstructure and compressive properties. *J. Mater. Res.* **22**, 314 (2007).
7. J.H. Han, K.B. Kim, S. Yi, J.M. Park, S.W. Sohn, T.E. Kim, D.H. Kim, J. Das, and J. Eckert: Formation of a bimodal eutectic structure in Ti-Fe-Sn alloys with enhanced plasticity. *Appl. Phys. Lett.* **93**, 141901 (2008).
8. D.V. Louzguine, L.V. Louzguina, H. Kato, and A. Inoue: Investigation of Ti-Fe-Co bulk alloys with high strength and enhanced ductility. *Acta Mater.* **53**, 2009 (2005).
9. J.M. Park, S.W. Sohn, D.H. Kim, K.B. Kim, W.T. Kim, and J. Eckert: Propagation of shear bands and accommodation of shear strain in the $\text{Fe}_{56}\text{Nb}_{4}\text{Al}_{40}$ ultrafine eutectic-dendrite composite. *Appl. Phys. Lett.* **92**, 091910 (2008).
10. J. Das, K.B. Kim, F. Baier, W. Löser, and J. Eckert: High-strength Ti-base ultrafine eutectic with enhanced ductility. *Appl. Phys. Lett.* **87**, 161907 (2005).
11. J.M. Park, D.H. Kim, K.B. Kim, and W.T. Kim: Deformation-induced rotational eutectic colonies containing length-scale heterogeneity in an ultrafine eutectic $\text{Fe}_{83}\text{Ti}_7\text{Zr}_6\text{B}_4$ alloy. *Appl. Phys. Lett.* **91**, 131907 (2007).
12. D.V. Louzguine, H. Kato, L.V. Louzguina, and A. Inoue: High-strength binary Ti-Fe bulk alloys with enhanced ductility. *J. Mater. Res.* **19**, 3600 (2004).
13. L. Shi, H. Ma, T. Liu, J. Xu, and E. Ma: Microstructure and compressive properties of chill-cast Mg-Al-Ca alloys. *J. Mater. Res.* **21**, 613 (2006).
14. J.M. Park, K.B. Kim, M.H. Lee, W.T. Kim, J. Eckert, and D.H. Kim: High strength ultrafine eutectic Fe-Nb-Al composites with enhanced plasticity. *Intermetallics* **16**, 642 (2008).
15. D.V. Louzguine, L.V. Louzguina, H. Kato, and A. Inoue: Investigation of high strength metastable hypereutectic ternary Ti-Fe-Co and quaternary Ti-Fe-Co-(V, Sn) alloys. *J. Alloys Compd.* **434-435**, 32 (2007).
16. J.M. Park, D.H. Kim, K.B. Kim, M.H. Lee, W.T. Kim, and J. Eckert: Influence of heterogeneities with different length scale on the plasticity of Fe-base ultrafine eutectic alloys. *J. Mater. Res.* **23**, 2003 (2008).
17. L.F. Mondolfo: *Aluminum Alloys: Structure and Properties* (Butterworths, London, UK 1976).
18. Y. Li, K. Georgarakis, S. Pang, J. Antonowicz, F. Charlot, A. Lemoulec, T. Zhang, and A.R. Yavari: AlNiY chill-zone alloys with good mechanical properties. *J. Alloys Compd.* **447**, 346 (2009).
19. B.A. Sun, M.X. Pan, D.Q. Zhao, W.H. Wang, X.K. Xi, M.T. Sandor, and Y. Wu: Aluminum-rich bulk metallic glasses. *Scr. Mater.* **59**, 1159 (2008).
20. T.T. Sasaki, T. Mukai, and K. Hono: A high-strength bulk nanocrystalline Al-Fe alloy processed by mechanical alloying and spark plasma sintering. *Scr. Mater.* **57**, 189 (2007).
21. P. Villars, A. Prince, and H. Okamoto: *Handbook of Ternary Alloy Phase Diagrams* (ASM International, Materials Park, OH, 1995).
22. JCPDFWIN: Version 2.2 (JCPDS, International Center for Diffraction Data, Newton Square, PA, 2001).
23. R. Elliott: *Eutectic Solidification Processing: Crystalline and Glassy Alloys* (Butterworths, London, UK, 1983).
24. K.A. Jackson and J.D. Hunt: Lamellar and rod eutectic growth. *Trans. Metall. Soc. AIME* **236**, 1129 (1966).
25. P.L. Ferrandini, F.L.G.U. Araujo, W.W. Batista, and R. Caram: Growth and characterization of the NiAl-NiAlNb eutectic structure. *J. Cryst. Growth* **275**, e147 (2005).
26. J.H. Han, K.B. Kim, S. Yi, J.M. Park, D.H. Kim, S. Pauly, and J. Eckert: Influence of a bimodal eutectic structure on the plasticity of $(\text{Ti}_{70.5}\text{Fe}_{29.5})_{91}\text{Sn}_9$ ultrafine composite. *Appl. Phys. Lett.* **93**, 201906 (2008).